

**Thermal transport in graphene junctions and quantum dots**Yong Xu,<sup>1</sup> Xiaobin Chen,<sup>1</sup> Jian-Sheng Wang,<sup>2</sup> Bing-Lin Gu,<sup>1</sup> and Wenhui Duan<sup>1,\*</sup><sup>1</sup>*Center for Advanced Study and Department of Physics, Tsinghua University, Beijing 100084, People's Republic of China*<sup>2</sup>*Center for Computational Science and Engineering and Department of Physics, National University of Singapore, Singapore 117542, Republic of Singapore*

(Received 19 January 2010; revised manuscript received 2 May 2010; published 20 May 2010)

Thermal-transport properties of various graphene junctions and quantum dots with nanoscale width are systematically investigated by nonequilibrium Green's-function method. Thermal conductance is insensitive to the detailed structure of the contact region but substantially limited by the narrowest part of the systems. Thermal-contact resistance in nanodevices carved entirely from graphene is quite low ( $\sim 10^{-10}$  m<sup>2</sup> K/W at 300 K), at least one order lower than that between graphene and other materials. Interestingly, thermal-contact resistance of double-interface junctions is just slightly higher than that of single-interface junctions, distinct from the case of electronic transport. Moreover, graphene junctions with smaller connection angles show lower thermal conductance but higher electronic conductance. The different, even opposite dependences of thermal- and electronic-transport properties on the structural characteristics may find wide applications in nanoelectronics and thermoelectricity.

DOI: [10.1103/PhysRevB.81.195425](https://doi.org/10.1103/PhysRevB.81.195425)

PACS number(s): 63.22.Rc, 65.80.Ck, 44.10.+i

**I. INTRODUCTION**

The studies of graphene have revealed a wealth of new physics and applications since it was first isolated experimentally in 2004.<sup>1</sup> One of the most fascinating and promising directions in current graphene research is its use as the base material to take the place of silicon for future nanoelectronics. In graphene-based nanoelectronics, junctions built by graphene nanoribbons (GNRs) and quantum dots (QDs) carved entirely from graphene are two major building blocks to achieve transistor action.<sup>2</sup> The advantage is that everything in electronics including conducting channels, quantum dots, barriers, electrodes, and interconnects can be patterned from graphene,<sup>2-4</sup> thus atomic perfect interfaces are naturally achieved and the contact resistances between the devices and electrodes are very low.<sup>5,6</sup> So far much research has focused on the electronic-transport properties of graphene-based nanodevices. Their thermal-transport properties, however, have not received enough attention they deserve.<sup>7,8</sup> In practice, heat dissipation in ever-smaller integrated circuits becomes more and more serious due to the increasing heat-generation rate per unit area and reduced thermal conduction induced by strong phonon boundary scattering.<sup>9</sup> Therefore, thermal design for individual nanodevice (such as junction and QD), as the basis for improvement of heat dissipation,<sup>10,11</sup> is of critical importance to the development of graphene-based nanoelectronics. Furthermore, the knowledge on thermal-transport properties will also be useful for the design and fabrication of high-performance thermoelectric devices.

Structural characteristics of graphene junctions and QDs, such as the contact geometry, width, edge shape, connection angle, and so on, significantly affect their electronic-transport properties.<sup>1,5,12-17</sup> Similarly, it is highly important to explore the influence of structural configuration on the thermal-transport properties of graphene junctions and QDs. Several theoretical works have been done on thermal transport in two-dimensional graphene sheet<sup>18-26</sup> and individual GNRs.<sup>27-32</sup> However, graphene-based nanodevices in realis-

tic situations have more complex structures, therefore their thermal-transport properties cannot be deduced solely from those of the regular graphene sheet or GNRs. To the best of our knowledge, the research on thermal transport in graphene junctions and QDs is still lacking. An investigation on how to tune thermal conductance of graphene-based nanodevices will be of practical interest and especially useful in the graphene device design.

In this work, we perform atomic-scale simulations on thermal transport in various graphene junctions and QDs with nanoscale width. The influence of their structural characteristics on thermal-transport properties is systematically investigated. It is found that thermal transport behaves quite differently from electronic transport. Thermal conductance of graphene junctions is insensitive to the detailed structure of the contact region and the width of the wide part of the structures but largely dependent on the width of the narrow part. Interestingly, thermal conductance of double-interface junctions is just slightly lower than that of single-interface junctions, and the connection angle and edge shape substantially affect thermal conductance of graphene junctions. Those unique effects of the structural characteristics on thermal conductance are very important for designing novel graphene-based junction devices. Due to very narrow constrictions and strong phonon scattering by the protruding parts, graphene QDs have much worse thermal-transport properties than graphene junctions, disadvantageous for the performance of QD electronic devices.

**II. METHOD**

Thermal conductance of graphene junctions and QDs is calculated by nonequilibrium Green's function (NEGF) method,<sup>33-36</sup> which is appropriate to deal with many-body problems with weak interactions and gives exact results if without many-body interactions. Since phonon mean-free path in graphene ( $\sim 775$  nm at room temperature)<sup>37</sup> is much longer than the size of graphene junctions or QDs considered

here, we neglect the phonon-phonon and electron-phonon interactions in our calculations. The second-generation reactive empirical bond order potential,<sup>38</sup> which was proved to give phonon modes of GNRs compatible with density-functional-theory calculations,<sup>39</sup> is employed to calculate force constants ( $\Phi$ ). Then, the Green's function and the phonon transmission function  $\Xi(\omega)$  are calculated as a function of frequency  $\omega$ , and finally thermal conductance  $\sigma(T)$  at different temperatures  $T$  can be obtained.

The transport system is divided into three parts: a finite center part (C) and two semi-infinite leads on the left (L) and right (R). The whole system has infinite numbers of freedom degrees. To make the problem solvable, the influence of leads is projected into the center through the self energies  $\Sigma_L(\omega)$  and  $\Sigma_R(\omega)$ . Then the retarded Green's function of the center part  $G_C^r(\omega)$  can be calculated by

$$G_C^r = [(\omega + i\delta)^2 - D_{CC} - \Sigma_L^r(\omega) - \Sigma_R^r(\omega)]^{-1}, \quad (1)$$

where  $\delta$  is a small broadening factor to prevent divergence during matrix inversion, and  $D_{CC}$  is the mass-weighted force constant matrix of the center part. The matrix element  $D_{ij} = \Phi_{ij} / \sqrt{M_i M_j}$ , where  $M_i$  is the mass of atom  $i$ , and  $\Phi_{ij}$  is the force constant between atom  $i$  and atom  $j$ . The retarded self-energies  $\Sigma_\alpha^r(\omega) = D_{Ca} g_\alpha^r(\omega) D_{aC}$  ( $\alpha = L, R$ ), where  $g_L^r(\omega)$  and  $g_R^r(\omega)$  are the retarded surface Green's functions of semi-infinite thermal leads, which can be calculated through decimation algorithm.<sup>40</sup> Once  $G_C^r(\omega)$  was calculated, the phonon transmission function  $\Xi(\omega)$  can be given by the Caroli formula

$$\Xi(\omega) = \text{Tr}[G_C^r(\omega)\Gamma_L(\omega)G_C^a(\omega)\Gamma_R(\omega)], \quad (2)$$

where  $G_C^a(\omega) = [G_C^r(\omega)]^\dagger$  is the advanced Green's function of the center part and  $\Gamma_\alpha(\omega) = i(\Sigma_\alpha^r(\omega) - [\Sigma_\alpha^r(\omega)]^\dagger)$  ( $\alpha = L, R$ ).

Thermal conductance can be obtained by the Landauer formula<sup>36</sup>

$$\sigma(T) = \frac{k_B^2 T}{2\pi\hbar} \int_0^\infty dx \frac{x^2 e^x}{(e^x - 1)^2} \Xi\left(\frac{k_B T}{\hbar} x\right), \quad (3)$$

where  $x = \hbar\omega / (k_B T)$ ,  $\hbar$  is the reduced Planck constant and  $k_B$  is the Boltzmann constant. The Landauer formula shows that thermal conductance is a weighted integral of the phonon-transmission function. Importantly, the weight factor  $[x^2 e^x / (e^x - 1)^2]$  decreases rapidly with increasing phonon frequency or decreasing temperature. This indicates that thermal conductance is mainly contributed by low-frequency phonons, especially at low temperatures. At very high temperatures (above 1000 K for graphene systems), the weight factor is close to 1 for all the available phonon frequencies, thus thermal conductance becomes saturated and approximately equals to the sum of phonon transmission. Thermal conductance contributed by electrons is not considered in our calculations. Since recent experiment showed that all sub-10-nm GNRs are semiconducting,<sup>17</sup> thermal conductance of GNRs narrower than 10 nm should be mostly dominated by phonons.

The phonon local density of states (LDOS) on the  $i$ th atom of the center part can also be given by the NEGF method

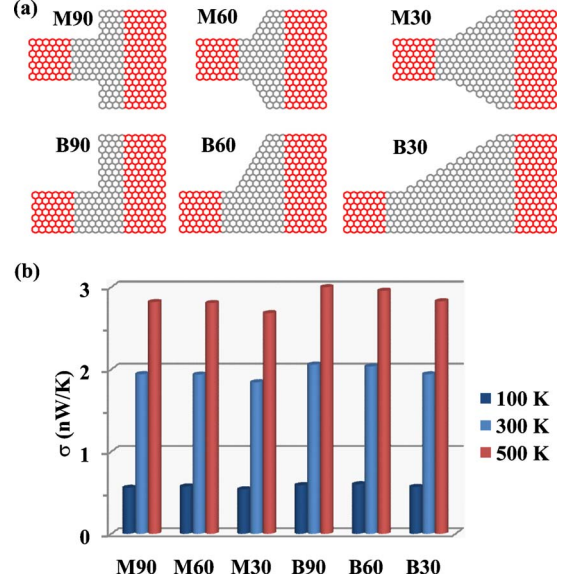


FIG. 1. (Color online) (a) Schematics of single-interface junctions constructed by connecting 8-ZGNR to the middle (labeled by “M90,” “M60,” and “M30”) or bottom (labeled by “B90,” “B60,” and “B30”) of 18-ZGNR. The number in the label (i.e., 30, 60, and 90) represents the angle between the edge of interface and that of 8-ZGNR. The red parts of the transport systems denote semi-infinite thermal leads (this convention is followed in all the figures). (b) Thermal conductance ( $\sigma$ ) at 100 K (dark blue), 300 K (blue), and 500 K (red) for the above six junctions. All the thermal conductances throughout this paper are in units of nano-Watt per Kelvin (nW/K).

$$\rho_i(\omega) = -\frac{2\omega}{\pi} \sum_{\alpha=x,y,z} \text{Im}[G_C^r(\omega)]_{i\alpha,i\alpha}. \quad (4)$$

Since the phonon LDOS directly displays the transport pathways for phonons with particular frequencies, it can provide valuable information to analyze the detailed transport mechanisms.

### III. RESULTS AND DISCUSSIONS

Single-interface junctions formed by connecting two GNRs have been demonstrated to be the basic device building blocks.<sup>5</sup> We first study the effect of contact geometry on thermal transport by considering various single-interface junctions as depicted in Fig. 1(a). Herein,  $n$ -ZGNR ( $n$ -AGNR) is used to denote a zigzag GNR (an armchair GNR) with  $n$  zigzag carbon chains (carbon dimer lines) across the ribbon width following the conventional notation. As shown in Fig. 1(b), thermal conductance of each junction increases monotonically from 100 to 500 K. Increasing temperature excites more phonons and opens new transport channels in high-frequency region, thus gives higher thermal conductance. More interestingly, thermal conductance of the junctions varies only slightly as the contact geometry changes, quite differently from the electronic-transport case where electronic conductance is significantly dependent on the detailed structure of the contact region.<sup>13-15</sup> This is fur-

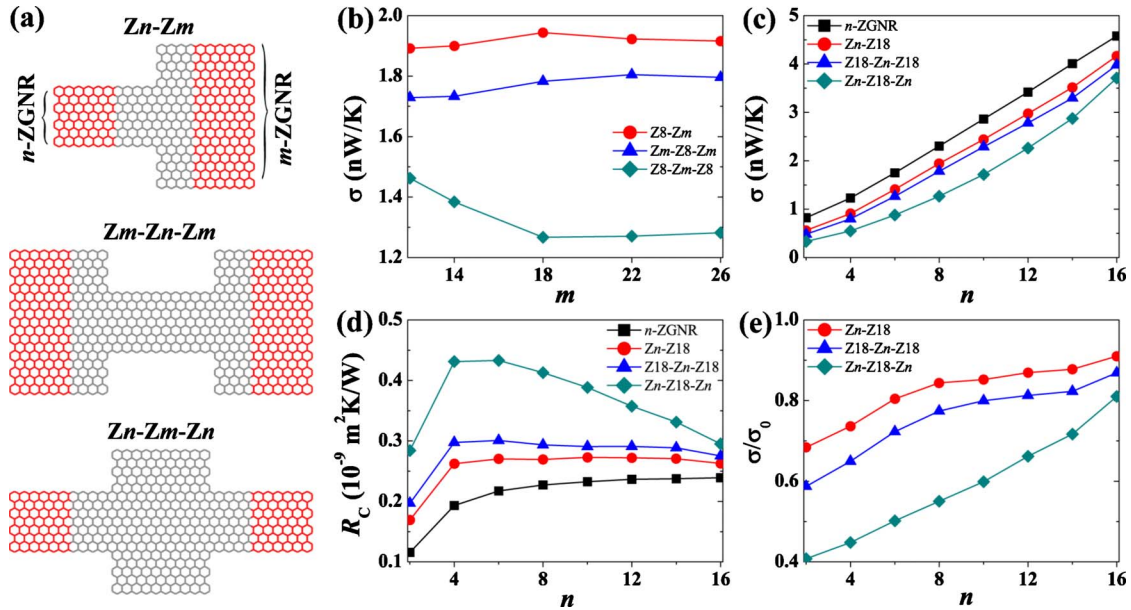


FIG. 2. (Color online) (a) Schematics of graphene junctions and quantum dots formed by  $n$ -ZGNR and  $m$ -ZGNR ( $n < m$ ): single-interface junction  $Z_n-Z_m$ , double-interface junction  $Z_m-Z_n-Z_m$ , and quantum dot  $Z_n-Z_m-Z_n$ . (b) Thermal conductance ( $\sigma$ ) at 300 K as a function of structure parameter  $m$  for “Z8- $Z_m$ ” (red circle), “ $Z_m$ -Z8- $Z_m$ ” (blue triangle), and “Z8- $Z_m$ -Z8” (cyan diamond). (c) Thermal conductance ( $\sigma$ ), (d) thermal contact resistance ( $R_c$ ) and (e) thermal conductance ratio ( $\sigma/\sigma_0$ ) at 300 K as a function of structure parameter  $n$  for pristine  $n$ -ZGNR (black square), “Zn-Z18” (red circle), “Z18-Zn-Z18” (blue triangle), and “Zn-Z18-Zn” (cyan diamond).

ther confirmed by investigating single-interface junctions composed of AGNRs (the data is not shown here). The distinct features of electronic and thermal transport can be explained from two aspects: (1) the typical length scales (e.g., wavelength and mean-free path) of phonons and electrons are different; (2) only electrons near the Fermi level contribute to electronic conductance while all phonon modes that are populated contribute to thermal conductance. Since thermal transport is insensitive to the detailed structure of the contact region, in the following we will focus on junctions with the contact geometry similar to “M90” in Fig. 1(a), where the ribbon width varies abruptly at the contact interface.

Figure 2(a) shows the single-interface junction, double-interface junction and QD formed by  $n$ -ZGNR and  $m$ -ZGNR ( $n < m$  is assumed without loss of generality). The double-interface junction was proposed as field effect transistor<sup>5</sup> and the QD presented here can be used for the controlled signal attenuation in graphene circuits.<sup>16</sup> For convenience, we use labels “ $Z_n-Z_m$ ”, “ $Z_m-Z_n-Z_m$ ”, and “ $Z_n-Z_m-Z_n$ ” to denote the above three types of systems, respectively, and then,  $n$  and  $m$ , respectively, correspond to the widths of the narrow and wide parts of the structures. The length of the center part in the transport direction is fixed in the following calculations since thermal conductance is found to only slightly change with the length.

It was previously observed that the ribbon width strongly influences the performance of graphene-based electronic nanodevices. For instance, the room temperature on/off ratio of GNR field-effect transistor induced by gate voltage increases exponentially as the ribbon width decreases.<sup>17</sup> Our results indicate that thermal-transport behavior even has a more complicated dependence on the ribbon widths of the

structures. As shown in Fig. 2(b), varying  $m$  (the width of the wide part) has little influence on thermal conductance of the single-interface and double-interface junctions [the upper and middle panels of Fig. 2(a)]. While, the wide part of the QD structure [the bottom panel of Fig. 2(a)] acts as a protrusion along the GNR and thermal conductance will first decrease with increasing width but become nearly constant for large width ( $m \geq 18$ ). In contrast, the width variation in the narrow part strongly affects thermal conductance of all the three types of graphene structures. As shown in Fig. 2(c), thermal conductance at 300 K of the single-interface and double-interface junctions is almost linearly proportional to the width of the narrow part while that of the QD approximately shows a quadratic dependence. Since the narrow part restricts the number of phonon transport channels, decreasing its width will remarkably reduce thermal conductance of the whole system.

Due to interface scattering, the junctions and QDs have lower phonon transmission and thermal conductance than the corresponding pristine narrow GNR (i.e.,  $n$ -ZGNR), as evidenced in Fig. 2(c). To quantitatively describe the effect of interface scattering, we define two quantities for graphene structures (junctions and QDs): thermal contact resistance  $R_c = W\delta/\sigma$ , which equals to the temperature difference between the two thermal leads per unit heat flux,<sup>41</sup> and thermal conductance ratio  $\sigma/\sigma_0$ , where  $W$  is the width of the narrower GNR,  $\delta = 0.335$  nm is chosen as the layer separation in graphite, and  $\sigma_0$  is the thermal conductance of perfect  $n$ -ZGNR. Thermal contact resistance and thermal conductance ratio at 300 K are presented as a function of  $n$  (the width of the narrow part) in Figs. 2(d) and 2(e). It can be seen that as  $n > 2$ , thermal contact resistance of the single-interface and double-interface junctions is nearly constant

while that of the QD approximately decreases linearly with  $n$ . This originates directly from the dependence of thermal conductance on the width of the narrow part [shown in Fig. 2(c)]. The irregularity appears at  $n=2$  due to predominant edge effect. Since thermal conductance of the two types of junctions is insensitive to the width of the wide part and the detailed structure of the contact region, their thermal contact resistance in fact corresponds to that of realistic graphene-based nanojunctions, or approximately equals to that between GNRs and graphene. Calculated thermal contact resistance between ZGNRs and graphene at 300 K is about  $0.3 \times 10^{-9} \text{ m}^2 \text{ K/W}$ , which is much lower than the values between graphene and silicon dioxide ( $5.6 \times 10^{-9} - 1.2 \times 10^{-8} \text{ m}^2 \text{ K/W}$ ).<sup>42</sup>

In practical applications, it is more useful to know thermal-conductance ratio ( $\sigma/\sigma_0$ ) rather than thermal conductance itself that is specific for particular systems. Thermal-conductance ratio is a measurement of thermal-transport properties for a series of systems with similar structures. As shown in Fig. 2(e), larger  $n$  always gives higher  $\sigma/\sigma_0$ . In detail, with increasing  $n$ ,  $\sigma/\sigma_0$  of the junctions experiences a quick increase when  $n$  is small, then rises very slowly as  $n > 8$ , but has a sharp increase when  $n$  is close to  $m$ ; while, that of QDs exhibits a nearly linear increase. The junctions show obviously better thermal-transport properties than the QDs. When the width of the narrow part is about 2 nm (i.e.,  $n=10$ ),  $\sigma/\sigma_0$  at 300 K are about 85%, 80%, and 60% for the single-interface junction, double-interface junction and QD, respectively.

As shown in Fig. 2(d), the single-interface junction always gives lower thermal contact resistance than its double-interface counterparts. This is easy to understand because one interface exerts less phonon scattering with respect to two interfaces. More interestingly, thermal contact resistance of the double-interface junction is just slightly higher than that of the single-interface junction, distinctly different from the electronic-transport behavior.<sup>16</sup> In contrast, the QD has obviously larger thermal contact resistance than the double-interface junction, though both of them have two interfaces. This seems to contradict with the common sense at the first glance. It is generally known when thermal resistances are connected in series, they are additive. The single interface produces additional thermal contact resistance with respect to the reference system (i.e., pristine  $n$ -ZGNR) as shown in Fig. 2(d), thus in fact acts as a thermal resistor. Two of them are placed in series in the double-interface junction and QD. The increase in thermal contact resistance with respect to the reference system in the double-interface junction/QD, however, is not equal to but lower/higher than two times that in the single-interface junction.

The conventional additive law fails when quantum interference effect plays an important role in transport.<sup>43</sup> Since thermal transport is phase coherent here, transport properties cannot be determined simply by the number of interfaces. A detailed comparison on phonon transmission will be helpful to understand the difference in calculated thermal conductance and thermal contact resistances. Figure 3(a) shows the phonon transmission of the transport systems composed of 8-ZGNR and 18-ZGNR. The phonon transmission function of the single-interface junction (Z8-Z18) is close to that of

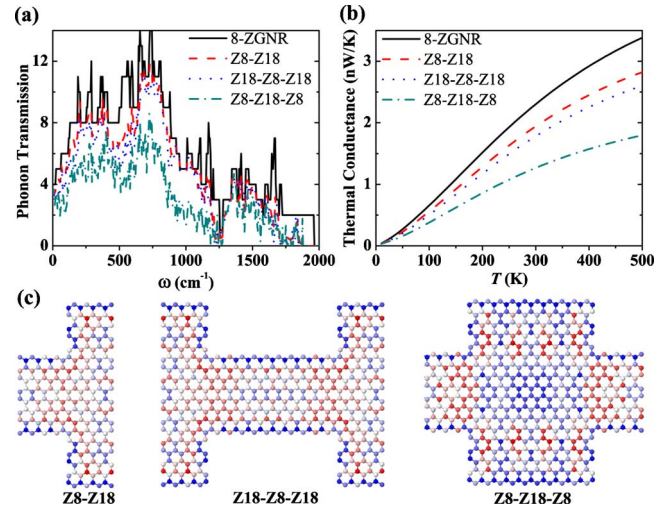


FIG. 3. (Color online) (a) Phonon transmission as a function of frequency  $\omega$  and (b) thermal conductance as a function of temperature  $T$  for pristine 8-ZGNR (black solid line), “Z8-Z18” (red dashed line), “Z18-Z8-Z18” (blue dotted line), and “Z8-Z18-Z8” (cyan dash-dotted line). (c) Schematics showing the phonon local density of states at  $\omega=900 \text{ cm}^{-1}$  for Z8-Z18, Z18-Z8-Z18, and Z8-Z18-Z8 structures. Red (blue) color represents the largest (smallest) value.

the narrow GNR (i.e., 8-ZGNR) but largely lower than that of the wide GNR (i.e., 18-ZGNR) (data not shown here). This shows that phonons from the narrow GNR experience little scattering when transporting across the interface into the wide GNR while phonons from the wide GNR are largely scattered as they transport into the narrow GNR. In other words, the average transmission per mode is direction-dependent due to the asymmetry structure of the single-interface junction. This can qualitatively explain the different transport properties of graphene junctions and QDs. Comparing with the single interface junction, the double-interface junction and QD [shown in Fig. 2(a)] have one more interface. To across this additional interface, phonons in the double-interface junction transmit from the narrow GNR into the wide GNR, different from those in the QD. Therefore, phonon scattering introduced by the second interface is small in the double-interface junction but large in the QD. As shown in Fig. 3(a), the phonon transmission of the double-interface junction (Z18-Z8-Z18) is slightly smaller than that of the single-interface junction (Z8-Z18) but apparently larger than that of the QD (Z8-Z18-Z8) in almost all the frequency range, especially when frequency is less than  $1200 \text{ cm}^{-1}$ . This leads to different thermal conductance as shown in Fig. 3(b): thermal conductance of the double-interface junction is only slightly lower than that of the single-interface junction but significantly higher than that of the QD in the whole temperature range (up to 500 K).

More detailed information on thermal transport can be obtained from the phonon LDOS, which gives the phonon distribution in real space.<sup>44</sup> Figure 3(c) shows the calculated phonon LDOS at  $\omega=900 \text{ cm}^{-1}$  for Z8-Z18, Z18-Z8-Z18, and Z8-Z18-Z8 structures. The corresponding transmission functions  $\Xi(\omega)$  are, respectively, 6.05, 5.27, and 2.62, less than the value of 7.00 for pristine 8-ZGNR. It can be seen from Fig. 3(c) that in the single-interface and double-

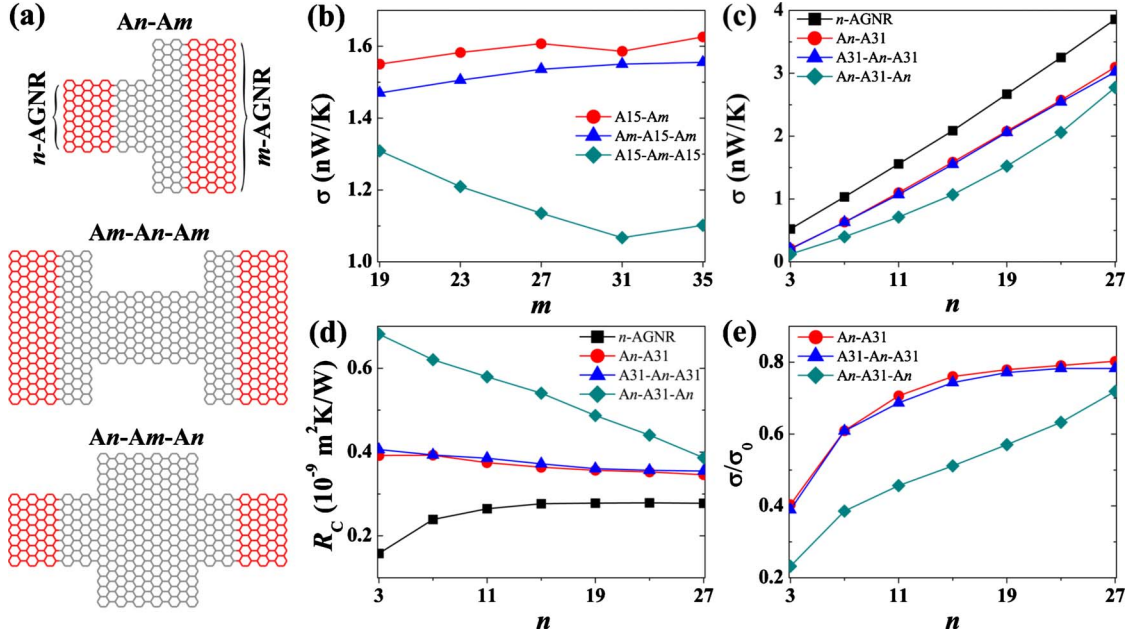


FIG. 4. (Color online) (a) Schematics of graphene junctions and quantum dots formed by  $n$ -AGNR and  $m$ -AGNR ( $n < m$ ): single-interface junction “ $An$ - $Am$ ,” double-interface junction “ $Am$ - $An$ - $Am$ ” and quantum dot “ $An$ - $Am$ - $An$ .” (b) Thermal conductance ( $\sigma$ ) at 300 K as a function of structure parameter  $m$  for “ $A15$ - $Am$ ” (red circle), “ $Am$ - $A15$ - $Am$ ” (blue triangle), and “ $A15$ - $Am$ - $A15$ ” (cyan diamond). (c) Thermal conductance ( $\sigma$ ), (d) thermal contact resistance ( $R_C$ ) and (e) thermal conductance ratio ( $\sigma/\sigma_0$ ) at 300 K as a function of structure parameter  $n$  for pristine  $n$ -AGNR (black square), “ $An$ - $A31$ ” (red circle), “ $A31$ - $An$ - $A31$ ” (blue triangle), and “ $An$ - $A31$ - $An$ ” (cyan diamond).

interface junctions, the atoms with large LDOS mainly distribute in the inner part of the structures and form straight channels along the transport direction, implying small reflection probability of phonons. While in the QD, large LDOS appears in the inner part of the narrow section and the protruding part of the wide section. Consequently, the phonons are easily scattered into the protruding part in the transport process. This explains why the QD has smaller phonon-transmission function than the junctions.

It is well known that the electronic-transport properties of AGNRs are significantly different from those of ZGNRs.<sup>1</sup> It will be interesting to explore the effect of edge shape on thermal-transport properties of graphene junctions and QDs, which is critical for their applications. In Fig. 4, we present thermal-transport properties of various junctions and QDs formed by AGNRs. It can be seen that the thermal-transport characteristics of the graphene junctions and QDs with armchair edges are very similar to those with zigzag edges but the structures with armchair edges have higher thermal contact resistance and lower thermal-conductance ratio. As shown in Fig. 4(d), thermal contact resistance of the junctions with armchair edges, which approximately equals to that between AGNRs and graphene, is about  $0.4 \times 10^{-9} \text{ m}^2 \text{ K/W}$  at 300 K. This is about 30% higher than that between ZGNRs and graphene. As shown in Fig. 4(e), thermal-conductance ratios at 300 K are about 77%, 76%, and 54% for the three types of systems depicted in Fig. 4(a) when the width of the narrow part is about 2 nm, which are sizably lower than the corresponding structures with zigzag edges. Our results indicate that zigzag edge gives better thermal-transport properties than armchair edge in graphene-based nanodevices. This is in accord with our previous

work,<sup>32</sup> which reveals an intrinsic anisotropy of thermal conductance in GNRs (i.e., thermal conductance per unit area of ZGNRs is up to  $\sim 30\%$  higher than that of AGNRs).

In practice, graphene junctions may be formed by GNRs with different connection angles (typically,  $30^\circ$ ,  $60^\circ$ ,  $90^\circ$ ,  $120^\circ$ , and  $150^\circ$ ).<sup>17,45</sup> In the following, we study thermal transport in various single-interface junctions patterned from graphene sheet [Fig. 5(a)], which are labeled according to the edge shape and connection angle of the composed GNRs (for instance, “ZA90” denotes a single-interface junction constructed by connecting ZGNR to AGNR with the connection angle of  $90^\circ$ ). Figure 5(b) shows thermal conductance as a function of temperature. It is found that the effect of the connection angle becomes larger as the temperature increases, and more importantly, the larger connection angle generally leads to higher thermal conductance at all these temperatures. Furthermore, we compare thermal-conductance ratio ( $\sigma/\sigma_0$ ) from 100 to 500 K in Fig. 5(c). The larger connection angle also results in higher  $\sigma/\sigma_0$ . For instance,  $\sigma/\sigma_0$  at 300 K of “ZZ120” is 78%, about 1.7 times that of “ZZ60.” In addition, graphene junctions with zigzag edge have higher  $\sigma/\sigma_0$  than those with armchair edge. The above results clearly indicate that graphene junctions with larger connection angles and zigzag edges exhibit better thermal transport properties. It should be noted that the connection angle has different influences on the transport behaviors of phonons and electrons. Larger connection angle introduces less phonon scattering for systems with different edges. In contrast, the effect of connection angle on electronic transport is much more complicated.<sup>16</sup> This is because electrons have more localized distribution and their transport is sensitive to the detailed structure. Interestingly, ZZ60 has

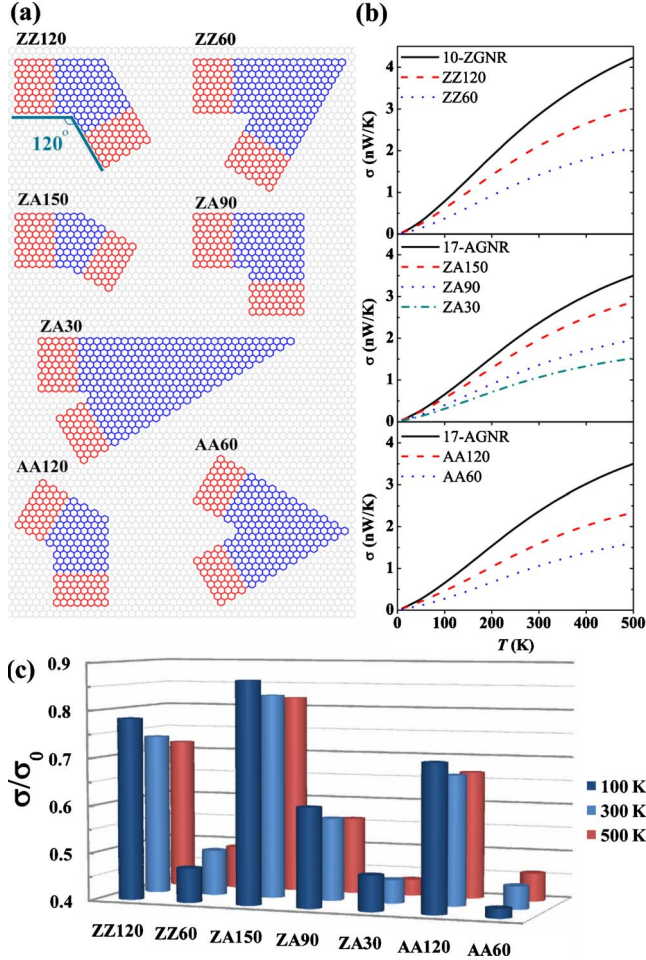


FIG. 5. (Color online) (a) Schematics of single-interface junctions formed by connecting 10-ZGNR and 17-AGNR, which have a similar width of  $\sim 2.0$  nm. The junctions can be classified into three categories in terms of the edge shape and connection angle: (1) “ZZ120” and “ZZ60;” (2) “ZA150,” “ZA90,” and “ZA30;” and (3) “AA120” and “AA60.” (b) Thermal conductance ( $\sigma$ ) as a function of temperature. (c) Thermal conductance ratios ( $\sigma/\sigma_0$ ) at 100 K (dark blue), 300 K (blue), and 500 K (red).

higher electronic conductance<sup>16</sup> but much lower thermal conductance than ZZ120. Thus junctions with small connection angles are hopefully used as thermoelectric devices.

Graphene QDs are believed to play an important role in quantum nanoelectronics.<sup>3</sup> Similar to the realistic model of graphene QD proposed in Ref. 3, we construct graphene QDs by carving narrow constrictions on 18-ZGNR as shown in Fig. 6(a). When the width of the narrow constrictions decreases, thermal conductance obviously decreases especially at high temperatures as presented in Fig. 6(b). The ratio ( $\eta$ ) between thermal conductance of the QD and that of pristine 18-ZGNR decreases rapidly as the temperature increases, and becomes nearly temperature independent when the temperature is higher than 100 K [Fig. 6(c)]. As expected, the QD with narrower constrictions has smaller  $\eta$ . Typically,  $\eta$  of “QD1” is less than 10% at 300 K due to the existence of very narrow constrictions. Since the narrow constrictions largely limit thermal conductance of QDs, especially at high temperatures, heat dissipation in QDs will be rather slow,

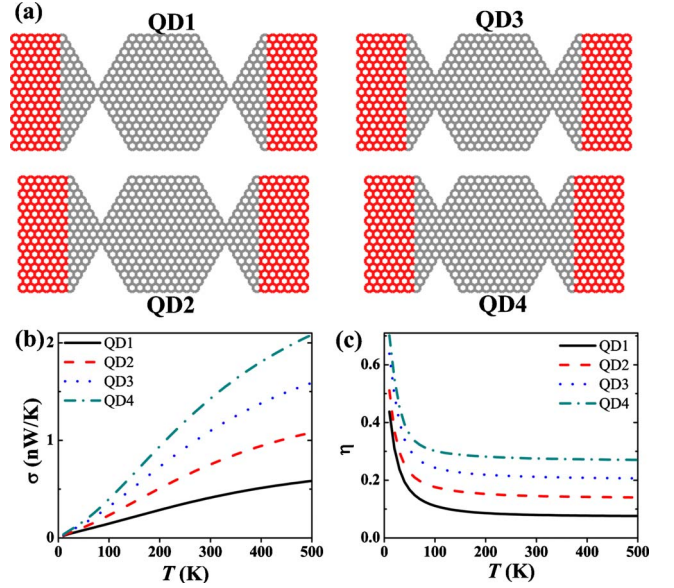


FIG. 6. (Color online) (a) Schematics of four graphene quantum dots carved from 18-ZGNR. The width of the narrow constrictions increases from QD1 to “QD4.” (b) Thermal conductance ( $\sigma$ ) and (c) thermal conductance ratio ( $\eta$ ) between quantum dots and pristine 18-ZGNR as a function of temperature.

which may degrade the performance of the graphene-based QD devices. On the other hand, the extremely low thermal conductance may significantly enhance the thermoelectric efficiency of QD structures.

#### IV. CONCLUSIONS

In summary, we have systematically studied thermal transport in various graphene junctions and QDs composed of GNRs with different widths, edge shapes, contact geometries and connection angles. It is found that the detailed structure of the contact region has little effect on thermal transport of graphene junctions although it may strongly influence electronic transport.<sup>13–15</sup> Thermal-transport properties of the graphene junctions are insensitive to the width of the wide part while decreasing the width of the narrow part will seriously reduce their thermal conductance. Thermal contact resistance is found to be very low in realistic graphene-based nanodevices, on the order of  $10^{-10}$  m<sup>2</sup> K/W at 300 K, much lower than that between graphene and other materials. Interestingly, thermal contact resistance of the double-interface junction is just slightly higher than that of the single-interface junction. Moreover, when the graphene junctions are formed by GNRs with different connection angles and edges, junctions with larger connection angles and zigzag edges exhibit better thermal-transport properties. Comparing with graphene junctions, graphene QDs generally show much worse thermal-transport properties because phonons are easily scattered into the protruding parts of QDs and the constrictions could be very narrow. This probably leads to the performance degradation of practical QD devices. Our work clearly reveals that thermal transport in graphene junctions and QDs has unique characteristics quite different from (even opposite to) those of electronic trans-

port. This indicates that thermal- and electronic-transport behaviors must be considered simultaneously when designing graphene-based nanoelectronic circuits, and also suggests the possibility to achieve high electronic conductance and low thermal conductance in some specific graphene junctions, which may be useful for applications in thermoelectricity.

## ACKNOWLEDGMENTS

This work was supported by the Ministry of Science and Technology of China (Grants No. 2006CB605105 and No. 2006CB0L0601), the National Natural Science Foundation of China, and the Ministry of Education of China.

\*Corresponding author; [dwh@phys.tsinghua.edu.cn](mailto:dwh@phys.tsinghua.edu.cn)

- <sup>1</sup>A. H. Castro Neto, F. Guinea, N. M. R. Peres, K. S. Novoselov, and A. K. Geim, *Rev. Mod. Phys.* **81**, 109 (2009), and references therein.
- <sup>2</sup>A. K. Geim and K. S. Novoselov, *Nature Mater.* **6**, 183 (2007).
- <sup>3</sup>R. M. Westervelt, *Science* **320**, 324 (2008).
- <sup>4</sup>L. A. Ponomarenko, F. Schedin, M. I. Katsnelson, R. Yang, E. W. Hill, K. S. Novoselov, and A. K. Geim, *Science* **320**, 356 (2008).
- <sup>5</sup>Q. Yan, B. Huang, J. Yu, F. Zheng, J. Zang, J. Wu, B.-L. Gu, F. Liu, and W. Duan, *Nano Lett.* **7**, 1469 (2007).
- <sup>6</sup>G. Liang, N. Neophytou, M. S. Lundstrom, and D. E. Nikonov, *Nano Lett.* **8**, 1819 (2008).
- <sup>7</sup>A. A. Balandin, S. Ghosh, W. Bao, I. Calizo, D. Teweldebrhan, F. Miao, and C. N. Lau, *Nano Lett.* **8**, 902 (2008).
- <sup>8</sup>M. Freitag, M. Steiner, Y. Martin, V. Perebeinos, Z. Chen, J. C. Tsang, and P. Avouris, *Nano Lett.* **9**, 1883 (2009).
- <sup>9</sup>E. Pop, S. Sinha, and K. E. Goodson, *Proc. IEEE* **94**, 1587 (2006).
- <sup>10</sup>D. G. Cahill, W. K. Ford, K. E. Goodson, G. D. Mahan, A. Majumdar, H. J. Maris, R. Merlin, and S. R. Phillpot, *J. Appl. Phys.* **93**, 793 (2003).
- <sup>11</sup>Y. Dubi and M. Di Ventra, [arXiv:0910.0425](https://arxiv.org/abs/0910.0425) (unpublished).
- <sup>12</sup>Z. Li, H. Qian, J. Wu, B.-L. Gu, and W. Duan, *Phys. Rev. Lett.* **100**, 206802 (2008).
- <sup>13</sup>X. Jia, M. Hofmann, V. Meunier, B. G. Sumpter, J. Campos-Delgado, J. M. Romo-Herrera, H. Son, Y.-P. Hsieh, A. Reina, J. Kong, M. Terrones, and M. S. Dresselhaus, *Science* **323**, 1701 (2009).
- <sup>14</sup>M. Yamamoto and K. Wakabayashi, *Appl. Phys. Lett.* **95**, 082109 (2009).
- <sup>15</sup>S. Hong, Y. Yoon, and J. Guo, *Appl. Phys. Lett.* **92**, 083107 (2008).
- <sup>16</sup>D. A. Areshkin and C. T. White, *Nano Lett.* **7**, 3253 (2007).
- <sup>17</sup>X. Li, X. Wang, L. Zhang, S. Lee, and H. Dai, *Science* **319**, 1229 (2008).
- <sup>18</sup>P. G. Klemens, *J. Wide Bandgap Mater.* **7**, 332 (2000).
- <sup>19</sup>P. G. Klemens, *Int. J. Thermophys.* **22**, 265 (2001).
- <sup>20</sup>N. Mingo and D. A. Broido, *Phys. Rev. Lett.* **95**, 096105 (2005).
- <sup>21</sup>K. Saito, J. Nakamura, and A. Natori, *Phys. Rev. B* **76**, 115409 (2007).
- <sup>22</sup>N. Bonini, M. Lazzeri, N. Marzari, and F. Mauri, *Phys. Rev. Lett.* **99**, 176802 (2007).
- <sup>23</sup>D. L. Nika, E. P. Pokatilov, A. S. Askerov, and A. A. Balandin, *Phys. Rev. B* **79**, 155413 (2009).
- <sup>24</sup>D. L. Nika, S. Ghosh, E. P. Pokatilov, and A. A. Balandin, *Appl. Phys. Lett.* **94**, 203103 (2009).
- <sup>25</sup>J.-W. Jiang, J.-S. Wang, and B. Li, *Phys. Rev. B* **79**, 205418 (2009).
- <sup>26</sup>B. D. Kong, S. Paul, M. B. Nardelli, and K. W. Kim, *Phys. Rev. B* **80**, 033406 (2009).
- <sup>27</sup>T. Yamamoto and K. Watanabe, *Phys. Rev. B* **70**, 245402 (2004).
- <sup>28</sup>J. Lan, J.-S. Wang, C. K. Gan, and S. K. Chin, *Phys. Rev. B* **79**, 115401 (2009).
- <sup>29</sup>E. Watanabe, S. Yamaguchi, J. Nakamura, and A. Natori, *Phys. Rev. B* **80**, 085404 (2009).
- <sup>30</sup>J. Hu, X. Ruan, and Y. P. Chen, *Nano Lett.* **9**, 2730 (2009).
- <sup>31</sup>Z. Guo, D. Zhang, and X.-G. Gong, *Appl. Phys. Lett.* **95**, 163103 (2009).
- <sup>32</sup>Y. Xu, X. Chen, B.-L. Gu, and W. Duan, *Appl. Phys. Lett.* **95**, 233116 (2009).
- <sup>33</sup>T. Yamamoto and K. Watanabe, *Phys. Rev. Lett.* **96**, 255503 (2006).
- <sup>34</sup>N. Mingo, *Phys. Rev. B* **74**, 125402 (2006).
- <sup>35</sup>Y. Xu, J.-S. Wang, W. Duan, B.-L. Gu, and B. Li, *Phys. Rev. B* **78**, 224303 (2008).
- <sup>36</sup>J.-S. Wang, J. Wang, and J. T. Lü, *Eur. Phys. J. B* **62**, 381 (2008).
- <sup>37</sup>S. Ghosh, I. Calizo, D. Teweldebrhan, E. P. Pokatilov, D. L. Nika, A. A. Balandin, W. Bao, F. Miao, and C. N. Lau, *Appl. Phys. Lett.* **92**, 151911 (2008).
- <sup>38</sup>D. W. Brenner, O. A. Shenderova, J. A. Harrison, S. J. Stuart, B. Ni, and S. B. Sinnott, *J. Phys.: Condens. Matter* **14**, 783 (2002).
- <sup>39</sup>M. Vandescoren, P. Hermet, V. Meunier, L. Henrard, and Ph. Lambin, *Phys. Rev. B* **78**, 195401 (2008).
- <sup>40</sup>F. Guinea, C. Tejedor, F. Flores, and E. Louis, *Phys. Rev. B* **28**, 4397 (1983).
- <sup>41</sup>E. T. Swartz and R. O. Pohl, *Rev. Mod. Phys.* **61**, 605 (1989).
- <sup>42</sup>Z. Chen, W. Jang, W. Bao, C. N. Lau, and C. Dames, *Appl. Phys. Lett.* **95**, 161910 (2009).
- <sup>43</sup>S. Datta, *Electronic Transport in Mesoscopic System* (Cambridge University Press, Cambridge, 1995).
- <sup>44</sup>M. Morooka, T. Yamamoto, and K. Watanabe, *Phys. Rev. B* **77**, 033412 (2008).
- <sup>45</sup>L. C. Campos, V. R. Manfrinato, J. D. Sanchez-Yamagishi, J. Kong, and P. Jarillo-Herrero, *Nano Lett.* **9**, 2600 (2009).